Dear Mr Liang,

As co-author of the article *Effect of differing stator and rotor radii on a three-class rotation-transmission nanobearing driven by a gigahertz rotary nanomotor*, we are pleased to let you know that the final version – containing full bibliographic details – is now available online.

To help you and the other authors access and share this work, we have created a Share Link – a personalized URL providing **50 days' free access** to the article. Anyone clicking on this link before January 19, 2020 will be taken directly to the final version of your article on ScienceDirect, which they are welcome to read or download. No sign up, registration or fees are required.

Your personalized Share Link:
https://authors.elsevier.com/c/1a98D8MvHgrDCO

Click on the icons below to share with your network:

Materials Today Communications 22 (2020) 100782

Contents lists available at ScienceDirect

Materials Today Communications

journal homepage: www.elsevier.com/locate/mtcomm

Effect of differing stator and rotor radii on a three-class rotation-transmission nanobearing driven by a gigahertz rotary nanomotor

Dong Liang, Zhen Xu, Zhongyu Fu, Wei Liao*

School of Mechanical and Automotive Engineering, Shanghai University of Engineering Science, Shanghai, 201620, China

ARTICLE INFO

Keywords:
Transmission system
Carbon nanotubes
Nanomotors
Nano-bearings
Molecular dynamics

ABSTRACT

Particularly critical for a transmission system is a control system that adjusts the output drive speed. Toward this end, we introduce herein a three-class rotation-transmission system. To obtain an effective down-converted rotation-transmission system, the coaxial rotary components are fabricated from carbon nanotubes (CNTs). At 300 K, a gigahertz nanomotor drives nanobearings and thereby changes the output rotation frequency. Considering the chirality of CNTs and the differing radii between stator and the rotor, 12 transmission models are established and tested by molecular dynamics simulations. The rotational-transmission ratio curves for the rotors give the dynamic response of the transmission systems. A down-converting transmission system is obtained when the radii of the stators and rotors differ by 0.3–0.4 nm. The dynamic response given by the rotational-transmission ratio curves for various models leads to useful conclusions about the design of such nanosystems.

1. Introduction

In carbon allotropes [1–3], carbon nanotubes (CNTs) behave similarly to graphene [4]. The two main characteristics of CNTs are that their in-plane strength is determined by the strength of the $2sp^2$-$2sp^2$ covalent bond, so the in-plane intensity is extremely high, ≈130 GPa [5], and the interfacial friction is extremely low. Due to the repulsion of π electrons in carbon atoms, adjacent graphene layers interact little between planes during sliding. In addition, the chirality of CNTs is determined by the helix angle at which the graphene sheets are rolled to produce a given CNT [6]. The chirality can be described by two chiral indices (n, m), and the unique properties of chirality give CNTs excellent mechanical properties, which have made CNTs popular for use in nanodevices. In addition, their tubular shapes have attracted significant research attention not only for fundamental science, but also because they have the potential to completely change nanodevices by enabling the fabrication of, for example, nanobearings [7–10], nano-oscillators [6,11–13], nanomotors [14–22], and nanotransmission systems [23–25].

With rotary nanomotors, the rotational frequency of the nanomotor typically exceeds the requirements of the device. To obtain a specific rotational frequency from a nanomotor, a nanosystem must transfer the input speed from the nanomotor to a given output speed (analogous to what is required of the drive train in a car). In 2015, Cai et al. [24,26,27] proposed a rotating transmission system for CNTs to transfer the magnitude and direction of motor rotation. In their model, a rotating CNT motor is linearly aligned coaxially to a rotor to form a rotation-transmission nanosystem. The rotor in the bearing is forced to rotate by the interaction between adjacent edges of the nanomotor. In 2018, Qiu et al. [28] proposed a two-stage rotation-transmission system based on CNTs that yielded a frequency-reducing transmission system. The system contains two coaxial multiwalled CNTs (i.e., first- and second-stage bearings). The motion of rotor 1 is constrained by adjacent CNTs, thereby minimizing its oscillation. The results show that, when the difference between the radii of the two rotors is greater than 0.18 nm and less than 0.34 nm, the rotation-transmission ratio (RTR) of rotor 2 is between 0.1 and 0.9. In 2019, Liang et al. [29] proposed a three-stage rotary transmission system based on CNTs, and their results showed that a decelerated transmission system can be obtained when the radii of the rotating parts are between 0.58 and 0.88 nm. However, the effect of the relationship between the rotating component and the stator on the output speed of the transmission system was not indicated.

To obtain a down-conversion transmission system that is more stable and controllable than previous models [26,30], we introduce herein a three-stage rotation-transmission system based on CNTs. The model has three coaxial nanobearings, which we call the first-, second-, and third-grade nanobearings. Since a rotor is constrained by adjacent components, the axial oscillation of the rotors during rotation is

* Corresponding author.
E-mail address: liaowei54@126.com (W. Liao).

https://doi.org/10.1016/j.mtcomm.2019.100782
Received 30 July 2019; Received in revised form 17 November 2019; Accepted 18 November 2019
Available online 20 November 2019

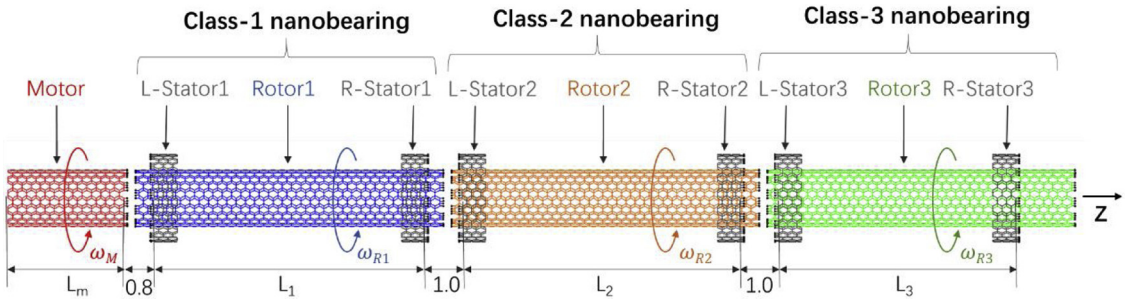

Fig. 1. Schematic illustration of a three-stage rotary transmission system (3-CRTS) made of CNTs. The system contains an input rotary motor and three bearings consisting of multi-walled CNTs [e.g., (1111) / (1717), where (1111) is a rotor and (1717) is a stator]. The CNTs are all aligned on the same axis, and all adjacent outer ends are hydrogenated. The initial gap between adjacent rotating members is 0.4 nm. The length of the motor is denoted L_m; other geometric parameters of the system are listed in Tables 1 and 2. ω_M is the rotational frequency of the input rotary motor, and ω_{R1}, ω_{R2}, and ω_{R3} are the output rotational frequencies of rotors 1, 2, and 3, respectively.

Table 1
Radii of CNTs in 3-CRTS involved in simulations. Dimensions are in nanometers.

CNT	(5,5)	(9,0)	(180)	(190)	(1010)	(1111)	(270)	(1616)	(260)
Radius	0.339	0.352	0.704	0.743	0.677	0.745	1.056	1.084	1.017
CNT	(280)	(290)	(1717)	(2121)	(300)	(310)			
Radius	1.095	1.134	1.152	1.423	1.173	1.212			

Table 2
Geometric parameters for 12 different 3-CRTS models used in simulations. Dimensions are in nanometers.

(a) Stators from the same zigzag CNT				
Model No.	1	2	3	4
Motor	(1111)	(1111)	(1111)	(1111)
Rotors	(1111)	(1111)	(1111)	(1111)
Stators	(270)	(280)	(290)	(300)
L_m/nm	3.074	3.074	3.074	3.074
L_1/nm	7.193	7.193	7.193	7.193
L_2/nm	7.393	7.393	7.393	7.393
L_3/nm	6.302	6.302	6.302	6.302
(a) Stators from the same armchair CNT				
Model No.	5	6	7	8
Motor	(1111)	(1111)	(190)	(190)
Rotors	(1111)	(1111)	(190)	(190)
Stators	(1616)	(1717)	(1616)	(1717)
L_m/nm	3.074	3.074	2.840	2.840
L_1/nm	7.193	7.193	7.365	7.365
L_2/nm	7.393	7.393	7.565	7.565
L_3/nm	6.302	6.302	6.302	6.302
(a) Stators from the same armchair CNT				
Model No.	9	10	11	12
Motor	(5,5)	(1616)	(9,0)	(260)
Rotors	(5,5)	(1616)	(9,0)	(260)
Stators	(1010)	(2121)	(180)	(350)
L_m (nm)	3.074	3.074	2.840	2.840
L_1 (nm)	7.193	7.193	7.365	7.365
L_2(nm)	7.393	7.393	7.565	7.565
L_3(nm)	6.302	6.302	6.302	6.302

suppressed. The motion of rotor 1 is constrained by its connection to the right edge of the motor and to the left edge of rotor 2 and by L-stator1 and R-stator1 (see Fig. 1). To show the feasibility and efficiency of rotation transmission, we also consider how the nanotube chirality affects the rotating parts and how the relative radii of rotor and stator affect the nanobearing functionality. Tables 1 and 2 list the relevant parameters. In addition, we explore various layouts of the three nanotubes in the nanosystem. Fig. 1 shows a detailed schematic diagram of the nanosystem, and Section 3 discusses the system dynamics response.

2. Model and methodology

2.1. Model of a three-class rotation-transmission system

Fig. 1 schematically illustrates a three-stage rotation-transmission system (3-CRTS) made entirely of CNTs. The radii of the CNTs are listed in Table 1, and Table 2 lists the parameters of the CNTs involved in the 12 models that were built and simulated for this study. In this work, all stators were 0.5 nm long. We study how the stators affect the rotation of the rotors from three viewpoints: first, we investigate how chirality affects the system by using armchair and zigzag CNTs for the rotating parts and stators, respectively. Second, the stators are made from armchair CNTs, and the rotors are made from either armchair or zigzag CNTs. Finally, the rotors and stators are made from CNTs with the same chirality.

3. Method

The interaction between atoms and adjacent components in the nanotransmission system is a bondless interaction described by the Lennard-Jones potential [31] cut off at 1.02 nm. The other parameters of the Lennard-Jones potential are σ_{C-C} = 0.34nm, ε_{C-C} = 2.8meV, ε_{H-H} = 1.5meV, σ_{H-H} = 0.265nm, σ_{C-H} = $(\sigma_{C-C} + \sigma_{H-H})/2$, and$\varepsilon_{C-H} = (\varepsilon_{C-C} + \varepsilon_{H-H})/2$. The interaction between carbon and hydrogen atoms is governed by the AIREBO potential. Because the outer edge of each stator and the adjacent edges of the rotating members are hydrogenated (i.e., each carbon atom is covalently bonded to a hydrogen atom [32]), the edge carbon atoms are saturated and, under normal conditions, do not bond with other hydrogen atoms. In a nanobearing, the rotor and stator radii differ by 0.30 to 0.43 nm. Thus, the rotors cannot escape the stators because of the stator edge barriers [33]. The direction of the axial forces exerted on the rotor can be varied during the simulation, but this has no effect on the results.

3.0.1. Rotation-transmission ratios

Each CNT is defined in the open-source molecular dynamics package LAMMPS [34] as a set of atoms that obey Newton's third law. In other words, each atom is assigned to a single block. The output

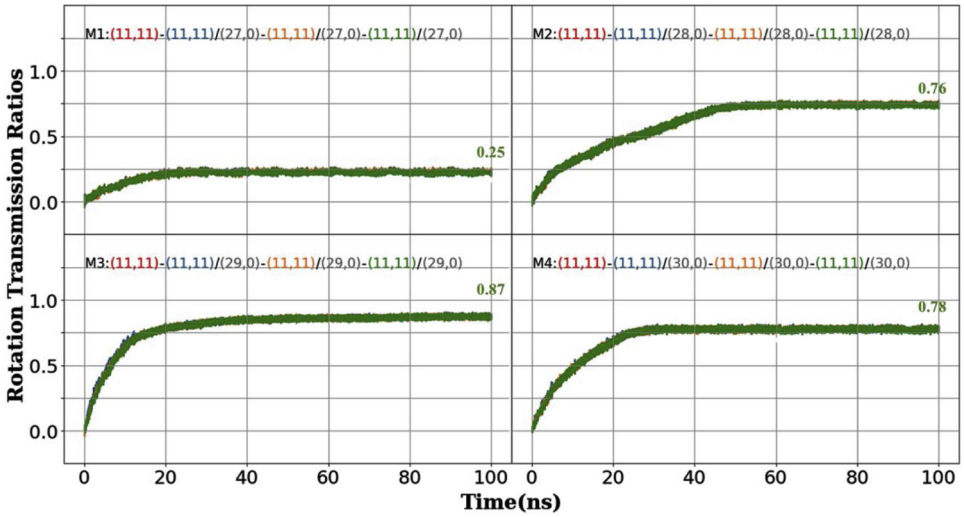

Fig. 2. Rotation transmission ratio as a function of time for rotors in the three-stage rotary transmission system driven by a motor with a 200 GHz input frequency at 300 K. M1–M4 indicate Model 1 to Model 4. The parameters are detailed in Fig. 1 and Tables 1 and 2. M1: (1111)- (1111)/ (270)- (1111)/ (270)- (1111)/ (270) indicates that, in Model 1, the components are all made of (11, 11) CNTs and the stators are made of (27, 0) CNTs. In each case, the blue, yellow, and green curves represent the RTRs for rotors 1–3, respectively. (For interpretation of the references to colour in this figure legend, the reader is referred to the web version of this article.)

rotational frequencies of the rotor are calculated by using

$$L = I \times \omega \tag{1}$$

where L is the angular-momentum vector of the block, I is the inertial tensor moment of the block, and ω is the angular velocity of the block. The calculation includes all effects due to the passage of atoms through the boundaries.

To quantify the efficiency of the rotation transmission of the three rotors in a system, the RTRs [28] are defined as follows:

$$R_1 = \frac{\omega_{R_1}}{\omega_M}, \quad R_2 = \frac{\omega_{R_2}}{\omega_M}, \quad R_3 = \frac{\omega_{R_3}}{\omega_M}, \tag{2}$$

where R_1, R_2, R_3 are the RTRs of rotors 1–3, ω_M, ω_{R_1}, ω_{R_2}, $\omega_{R_3}$are the angular velocities of the motor and rotors 1–3, respectively.

The efficiency of the rotation transmission is categorized into three levels [30],

(a) $R_3 < 0.1$ or $R_3 > 0.9$, transmission fails:

After 20 ns of rotation, if R_3 is less than 0.1 or greater than 0.9, the deceleration transmission has failed.

(a) $0.1 < R_3 < 0.4$ or $0.6 < R_3 < 0.9$, transmission is possible:

After 20 ns of rotation, if R_3 is less than 0.4 and greater than 0.1 or less than 0.9 and greater than 0.6, the transmission is acceptable.

(a) $0.4 < R_3 < 0.6$, excellent transmission:

After 20 ns of rotation, if R_3 is between 0.4 and 0.6, then the system provides ideal down-converted rotation transmission.

The mass centers X_{R_1}, X_{R_2}, X_{R_3} of rotors 1–3 are given as a function of time as

$$X_{R_1}(t) = \frac{\sum_{n_1} m_i X_i(t)}{\sum_{n_1} m_i}, \quad X_{R_2}(t) = \frac{\sum_{n_2} m_i X_i(t)}{\sum_{n_2} m_i}, \quad X_{R_3}(t) = \frac{\sum_{n_3} m_i X_i(t)}{\sum_{n_3} m_i} \tag{3}$$

where n_1, n_2, and n_3 are the number of atoms in rotors 1–3, respectively, and m_i and X_{R_i} are the mass and x coordinate of atom i, respectively.

3.0.2. Details for molecular dynamics simulations

The simulation was done with LAMMPS [35]. The atomic integration of Newton's second law in the system used a 1 fs time step and a maximum number of iterations of 100 million. The system configuration was readjusted by minimizing the system energy. Next, all the stators were fixed, and the hydrogen atoms on the stators were relaxed. Carbon atoms 0.5 nm from the left end of the rotating parts were constrained by a spring force in the x, y, and z directions. A Nosé-Hoover thermal bath was continuously simulated in the standard *NVT* ensemble with a time step of 200 ps. The left edge of the motor was constrained in the z direction and the motor started rotating at 200 GHz after canceling the constraints of the rotating components and the thermal bath. The rotors were released from their fixed degrees of freedom. The temperature of the system was controlled by using a Nosé-Hoover thermostat [36] set at 300 K for 20 or 100 ns. The results of the simulation after 200 iterations were averaged, and the average was recorded for further analysis.

4. Simulation results and discussion

4.1. Stators made of zigzag carbon nanotubes

In the rotation-transmission models M1–M4, the motor and rotors 1–3 are each made from armchair CNTs, and the stators are each made of zigzag CNTs. To better characterize the rotation transmission for each model, Fig. 2 shows the RTRs as functions of time for rotors 1–3 for the four models.

In Models M1(see Movie S1 in the Supplementary Materials), M2, and M3, the motor and rotors 1–3 are made of armchair CNTs, and the rotor and stator radii differ by 0.3 to 0.4 nm. The difference in radius between the rotor and the stator in Models 1–3 is 0.331, 0.350, and 0.389 nm, respectively. Because the CNTs in each model are arranged concentrically, the RTR of the rotor increases with increasing difference in radius between rotor and stator. In the nanobearings, a stator whose radius differs only slightly from its rotor interacts strongly with the rotor via van der Waals forces, so that the rotor is strongly constrained in both the axial and radial directions. Therefore, we conclude that a usable down-converting transmission system may be obtained when the stator radius is only 0.3–0.4 nm greater than the rotor radius.

In Model M4 (see Movie S2 in the Supplementary Materials), the rotor has a RTR about 0.78 less than the rotor in Model M3 (for which RTR = 0.87). This is because the stator radius is 0.428 nm greater than the rotor radius, which exceeds the 0.4 nm gap between adjacent rotating parts. The constraint exerted by the stator on the rotor is weaker than that of the adjacent rotating parts, thereby increasing the oscillation amplitude of the rotor. Therefore, we conclude that an excellent down-converted rotational transmission system can be obtained when the rotor and stator radii differ by 0.4 to 0.5 nm.

Note that, in Models M1 and M4, the difference in radius between

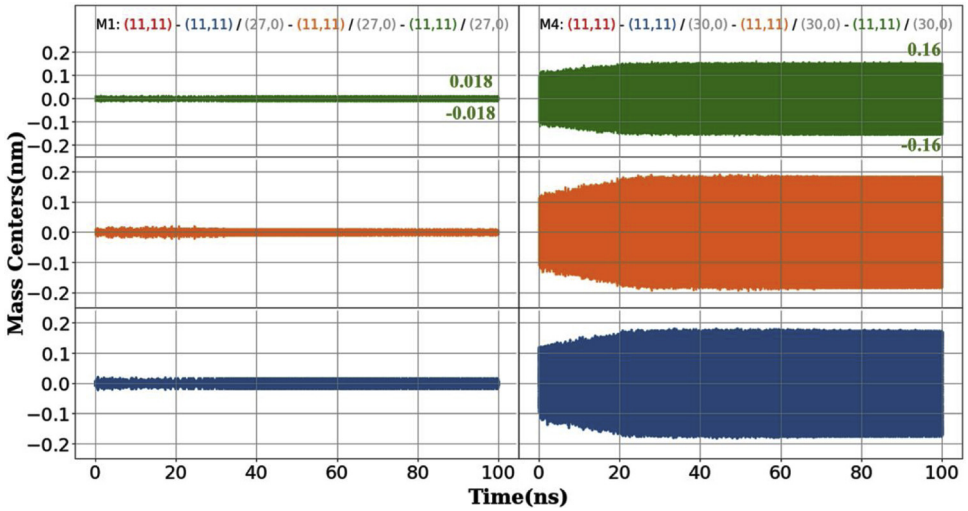

Fig. 3. Center-of-mass position as a function of time for three rotors rotating in M1 and M4. Blue, yellow, and green curves represent rotors 1–3, respectively. (For interpretation of the references to colour in this figure legend, the reader is referred to the web version of this article.)

rotor and stator is 0.331 and 0.428 nm, respectively. Although the difference in radius between the rotor and stator of Model M1 and between the rotor and stator of Model M4 is only 0.097 nm, the amplitude of the oscillation in the radial direction in Model M4 is an order of magnitude greater than that in Model M1. For example, in Fig. 3, the radial amplitude of the center of mass of rotor 3 in Model M1 is 0.018 nm, whereas the center of mass of rotor 3 in Model M4 is 0.16 nm.

4.2. Stators made of armchair carbon nanotubes

To explore the interaction between different chiral CNTs and obtain a functional three-stage rotary transmission system with reduced rotation frequency, the rotating parts in the simulation are made of zigzag or armchair CNTs, and the stators are made of armchair CNTs. Fig. 3 shows the RTRs as a function of time for rotors 1–3.

When the radius of the stator is 0.3 to 0.5 nm greater than that of the rotor, the RTR can be obtained. For example, in Models M5–M8 in Fig. 4, the stators for the bearings are all made of armchair CNTs, and the stator radii are 0.33 to 0.41 nm greater than the radii of the corresponding rotors. In models M5 and M6, the rotating parts are made of armchair CNTs, and the RTRs of the rotors in M5 are slightly greater than those for the rotors in M6. In Models M7 and M8, the rotating parts are all made of zigzag CNTs, and the RTRs of the rotors in M7 are slightly greater than those for the rotors in M8. These results occur because the stator radii in M5 and M7 are 0.3 to 0.4 nm greater than the rotor radii, whereas the stator radii are more than 0.4 nm greater than the rotor radii in M6 and M8.

Bearings made of armchair-CNT stators and zigzag-CNT rotors thus lead to transmission systems with smaller RTRs than bearings made of armchair CNTs. For example, compare the results of (i) Models M5 and M7 with (ii) M6 and M8 in Fig. 4. These results occur because the potential barriers of armchair CNTs distribute evenly in the generatrix direction, whereas those of the zigzag CNT do so in the circumferential direction [37]. Therefore, the armchair-CNT rotor of Models M7 and M8 experience more friction when associated with zigzag-CNT stators.

4.3. Stators and rotors with the same chirality

A three-stage rotary drive model can rotate when the difference between stator and rotor radii is between 0.3 and 0.4 nm. In Models M9 and M10, both rotors and stators are made of armchair CNTs, and the minimum difference between the rotor and stator radii is 0.338 nm. In M11 and M12, both rotors and stators are made of zigzag CNTs, and the minimum difference between rotor and stator radii is 0.352 nm. Fig. 5 shows the RTRs as a function of time for rotors 1–3 in Models M9–M12.

When both the rotating parts and the stators are made of armchair CNTs, and the radius of the stators is about 0.4 nm greater than that of the rotor, the RTR decreases with increasing radius of the nanobearing.

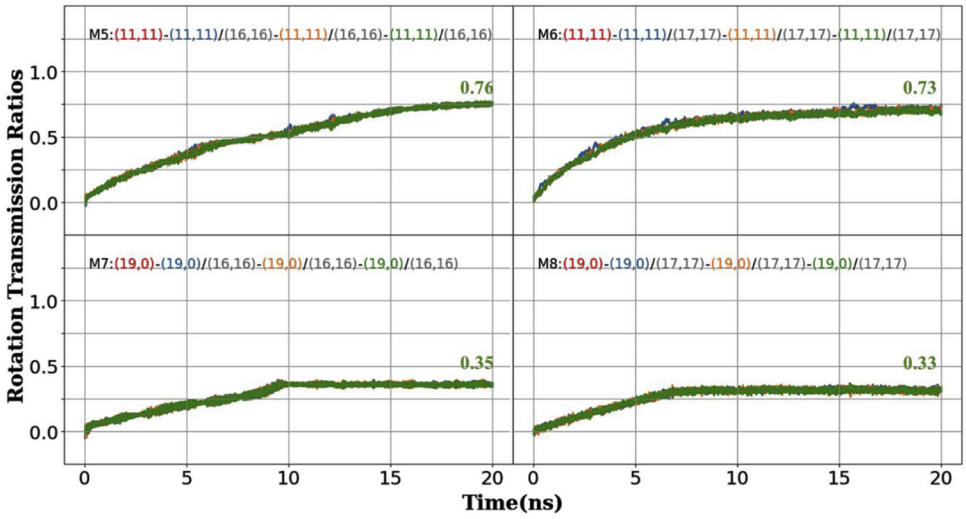

Fig. 4. Rotation transmission ratio as a function of time for rotors in a three-stage rotary transmission system driven by a motor with 200 GHz input frequency at 300 K. M5–M8 indicate Model M5 to Model M8. The parameters are listed in Fig. 1 and Tables 1 and 2. M7: (190)- (190)/ (1616)- (190)/ (1616)- (190)/ (1616) indicates that, in Model M7, the rotors are made of (19, 0) CNTs and the stators are made of (16, 16) CNTs. In each case, the blue, yellow, and green curves represent the RTRs for rotors 1–3, respectively. (For interpretation of the references to colour in this figure legend, the reader is referred to the web version of this article.)

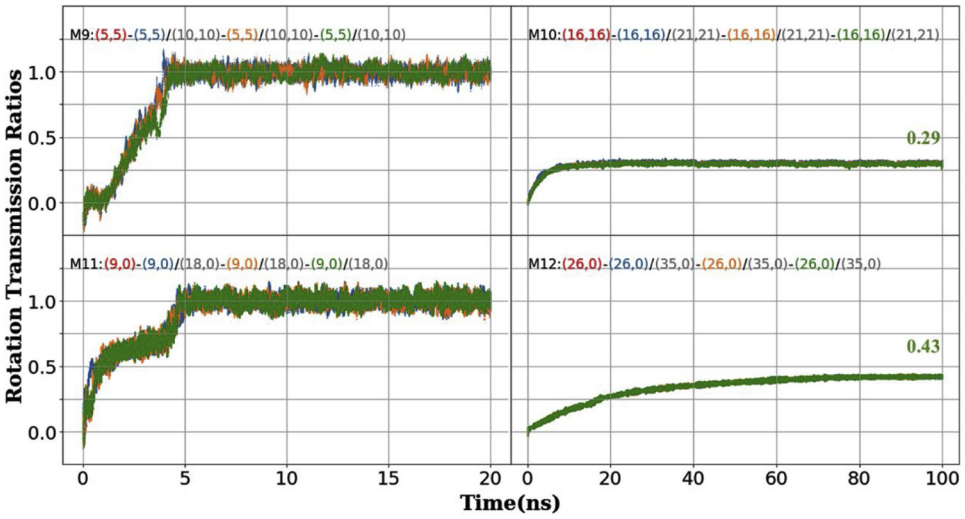

Fig. 5. Rotation transmission ratio as a function of time for rotors in three-stage rotary transmission system driven by a motor with 200 GHz input frequency at 300 K. M9–M12 indicate Model M9 to Model M12. The parameters are listed in Fig. 1 and Tables 1 and 2. M9: (5,5)- (5,5)/ (1010)- (5,5)/ (1010)-(5,5)/ (1010) indicates that, in Model M9, the rotors are made of (5,5) CNTs and the stators are made of (1010) CNTs. In each case, the blue, yellow, and green curves represent the RTR of rotors 1–3, respectively. (For interpretation of the references to colour in this figure legend, the reader is referred to the web version of this article.)

See, for example, Model M9 in Fig. 5, M5 in Fig. 3, and M10 in Fig. 5, where the rotor RTRs are 1.0, 0.76, and 0.29, respectively. Therefore, we conclude that a usable frequency-reducing rotary transmission system is obtained with a stator radius 0.3 to 0.4 nm greater than the rotor radius and with a radius of 0.7–1.0 nm for the rotating parts.

In Models M11 and M12 (Fig. 5), both the rotating parts and stators are made of zigzag CNTs. When the radius of the stator is 0.3 to 0.4 nm greater than that of the rotor, the transmission ratio of the rotor decreases with increasing nanobearing radius. This is the same phenomenon exhibited by nanobearings made entirely of armchair CNTs.

In Models M9 and M11 (Fig. 5), the rotors made of the smaller-radius CNTs rotate synchronously with the motor. However, as shown in Fig. 6, the rotors bend and deform during rotation. Note that the degree of deformation of rotors 1–3 decreases from left to right. Thus, shortening the rotors in the model should decrease the degree of bending.

5. Conclusions

We simulate at 0 and 100 ns a three-stage rotary transmission system powered by a 200 GHz motor and operated at a constant temperature of 300 K. The simulation allows us to test 12 configurations of CNT chirality of the rotating component and of stators and rotors of different radii. By modeling a rotation-transmission system composed of CNTs of varying chirality, we obtain an effective down-conversion rotation-transmission system. The rotor RTRs for the different models lead to the following conclusions regarding the nanostructure design:

(i) When the rotating parts and stators are both made of zigzag CNTs and the stator radii are 0.3 to 0.4 nm greater than the rotor radii, the simulation produces excellent down-conversion transmission systems.

(ii) When the stators are made of armchair CNTs, the rotors are made of zigzag or armchair CNTs, and the stator radii are 0.3 to 0.5 nm greater than the rotor radii, the model may be considered as an available design option.

(iii) Because the armchair CNTs result in greater friction on the zigzag-shaped CNTs, bearings composed of armchair-CNT stators and zigzag-CNT rotors more effectively reduce the output rotation frequency of the rotor.

(iv) When the stator radii are 0.3 to 0.4 nm greater than the rotor radii and the radius of the rotating parts is 0.7–1.0 nm, the simulation produces a usable frequency-reduction rotation-transmission system.

(v) Increasing the difference in radius between the stators and rotors by 0.1 nm significantly increases the amplitude of the radial oscillation of the rotors.

Supplementary materials

The following are available online at https://github.com/ld269440877/Micromachines Supplementary Materials/tree/master/S1,
Figure S1: M1-motor&Rotor1111Stator270_close20ns.png,
Video S1: M1-motor&Rotor1111Stator270_close20ns.mp4.

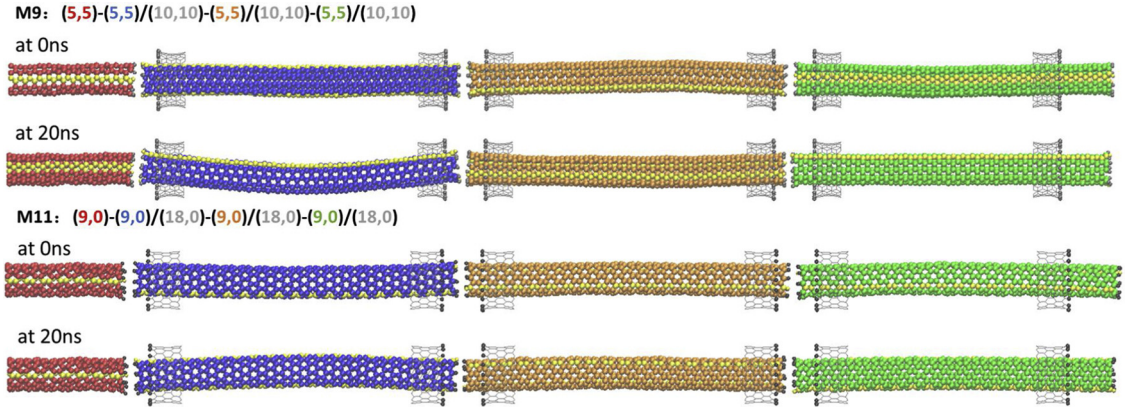

Fig. 6. Simulation of Models M9 and M11 at $t = 0$ and 20 ns. In each model, red, blue, yellow, and green CNTs from left to right represent the motor and rotors 1–3, respectively (Multimedia view). (For interpretation of the references to colour in this figure legend, the reader is referred to the web version of this article.)

Figure S2: M4-motor&rotors1111Stators300_close20ns.png,
Video S2: M4-motor&rotors1111Stators300_close20ns.mp4.

Data availability statement

The raw data required to reproduce these findings are available to download from
git@github.com:ld269440877/Micromachines_Supplementary_Materials.git.
The processed data required to reproduce these findings are available to download from
git@github.com:ld269440877/Micromachines_Supplementary_Materials.git.

Credit author statement

Z.X. proposed and supervised the project. D.L. designed and performed the experiments and wrote the manuscript. Z.Y.F. co-supervised the project and participated in data analysis.

Author contributions

Z.X. and W.L. proposed and supervised the project. D.L. designed and performed the experiments and wrote the manuscript. Z.Y.F. co-supervised the project and participated in data analysis.

Funding

This research was funded by the National Science Foundation of China, grant number 11,604,203.

Conflicts of Interest

The authors declared that they have no conflicts of interest to this work. We declare that we do not have any commercial or associative interest that represents a conflict of interest in connection with the work submitted.

Acknowledgment

This work was supported by the National Science Foundation of China and the National Supercomputing Center in Shenzhen.

Appendix A. Supplementary data

Supplementary material related to this article can be found, in the online version, at doi:https://doi.org/10.1016/j.mtcomm.2019.100782.

References

[1] H.W. Kroto, J.R. Heath, S.C. O'Brien, et al., C60: Buckminsterfullerene, Nature 318 (1985) 162–163.
[2] J.-W. Jiang, J. Leng, J. Li, et al., Twin graphene: A novel two-dimensional semiconducting carbon allotrope, Carbon 118 (2017) 370–375.
[3] K. Cai, L. Wang, Y.M. Xie, Buckling behavior of nanotubes from diamondene, Mater. Des. 149 (5) (2018) 34–42.
[4] K.S. Novoselov, A.K. Geim, S.V. Morozov, et al., Electric field effect in atomically thin carbon films, Science 306 (5696) (2004) 666–669.
[5] S. Iijima, Helical microtubules of graphitic carbon, Nature 354 (6348) (1991) 56–58.
[6] W. Guo, Y. Guo, H. Gao, et al., Energy dissipation in gigahertz oscillators from multiwalled carbon nanotubes, Phys. Rev. Lett. 91 (12) (2003) 125501.
[7] J. Shi, K. Cai, L.N. Liu, et al., Conditions for escape of a rotor in a rotary nanobearing from short triple-wall nanotubes, Sci. Rep. 8 (2018) 913.
[8] Jw. Kang, H.J. Hwang, Nanoscale carbon nanotube motor schematics and simulations for micro-electro-mechanical machines, Nanotechnology 15 (2004) 1633–1638.
[9] V.V. Deshpande, H.Y. Chiu, H.W.C. Postma, Carbon nanotube linear bearing nanoswitches, Nano Lett. 6 (2006) 1092–1095.
[10] C. Zhu, W. Guo, T. Yu, Energy dissipation of high-speed nanobearings from double-walled carbon nanotubes, Nanotechnology 19 (46) (2008) 465703.
[11] Q. Zheng, Q. Jiang, Multiwalled carbon nanotubes as gigahertz oscillators, Phys. Rev. Lett. 88 (8) (2002) 045503.
[12] S.B. Legoas, V.R. Coluci, S.F. Braga, et al., Molecular-dynamics simulations of carbon nanotubes as gigahertz oscillators, Phys. Rev. Lett. 90 (5) (2003) 055504.
[13] K. Cai, H. Yin, Q.H. Qin, et al., Self-excited oscillation of rotating double-walled carbon nanotubes, Nano Lett. 14 (5) (2014) 2558–2562.
[14] A.M. Fennimore, T.D. Yuzvinsky, W.-Q. Han, et al., Rotational actuators based on carbon nanotubes, Nature 424 (2003) 408–410.
[15] J.W. Kang, H.J. Hwang, Nanoscale carbon nanotube motor schematics and simulations for micro-electro-mechanical machines, Nanotechnology 15 (11) (2004) 1633–1638.
[16] C. Zhu, W. Guo, T. Yu, Energy dissipation of high-speed nanobearings from double-walled carbon nanotubes, Nanotechnology 14 (46) (2008) 465703.
[17] B. Wang, L. Vuković, P. Král, Nanoscale rotary motors driven by electron tunneling, Phys. Rev. Lett. 101 (2008) 186808.
[18] A. Barreiro, R. Rural, E.R. Hernández, et al., Subnanometer Motion of Cargoes Driven by Thermal Gradients Along Carbon Nanotubes, Science 320 (5877) (2008) 775–778.
[19] H.A. Zambrano, J.H. Walther, R.L. Jaffe, Thermally driven molecular linear motors: A molecular dynamics study, J. Chem. Phys. 131 (24) (2009) 241104.
[20] M. Hamdi, A. Subramanian, L. Dong, et al., Simulation of rotary motion generated by head-to-head carbon nanotube shuttles, IEEE/ASME Trans. 18 (1) (2013) 130–137.
[21] K. Cai, J. Yu, J. Wan, et al., Configuration jumps of rotor in a nanomotor from carbon nanostructures, Carbon 101 (2016) 168–176.
[22] K. Cai, J. Yu, L. Liu, et al., Rotation measurements of a thermally driven rotary nanomotor with a spring wing, Phys. Chem. Chem. Phys. 18 (2016) 22478–22486.
[23] K. Cai, H. Cai, L. Ren, et al., Over-speeding rotational transmission of a carbon nanotube-based bearing, J. Phys. Chem. C 120 (2016) 5797–5803.
[24] K. Cai, H. Yin, N. Wei, et al., A stable high-speed rotational transmission system based on nanotubes, Appl. Phys. Lett. 106 (2) (2015) 021909.
[25] H.A. Zambrano, J.H. Walther, R.L. Jaffe, Thermally driven molecular linear motors: a molecular dynamics study, J. Chem. Phys. 131 (24) (2009) 241104.
[26] K. Cai, H. Yin, N. Wei, et al., A stable high-speed rotational transmission system based on nanotubes, Appl. Phys. Lett. 106 (2) (2015) 021909.
[27] K. Cai, H. Cai, J. Shi, et al., A nano universal joint made from curved double-walled carbon nanotubes, Appl. Phys. Lett. 106 (24) (2015) 241907.
[28] W. Qiu, J. Shi, Z. Cao, et al., A two-class rotation transmission nanobearing driven by gigahertz rotatry, Comput. Mater. Sci. 154 (2018) 97–105.
[29] D. Liang, Z. Fu, Z. Xu, A three-stage rotary transmission nanobearing driven by a gigahertz nanomotor, AIP Adv. 9 (10) (2019).
[30] W. Qiu, J. Shi, Z. Cao, et al., A two-class rotation transmission nanobearing driven by gigahertz rotary nanomotor, Comput. Mater. Sci. 154 (2018) 97–105.
[31] J.E. Jones, On the determination of molecular fields. Ii. From the equation of state of a gas, Proc. R. Soc. A 106 (738) (1924) 463–477.
[32] S.J. Stuart, A.B. Tutein, J.A. Harrison, A reactive potential for hydrocarbons with intermolecular interactions, J. Chem. Phys. 112 (14) (2000) 6472–6486.
[33] Z. Guo, T. Chang, X. Guo, et al., Thermal-induced edge barriers and forces in interlayer interaction of concentric carbon nanotubes, Phys. Rev. Lett. 107 (10) (2011) 105502.
[34] S. Plimpton, Fast parallel algorithms for short-range molecular dynamics, J. Comput. Phys. 117 (1995) 1–19.
[35] Lammps. https://lammps.sandia.gov/., 2019.
[36] S. Nosé, A molecular dynamics method for simulations in the canonical ensemble, Mol. Phys. 52 (2) (1984) 255–268.
[37] R. Saito, R. Matsuo, T. Kimura, Anomalous potential barrier of double-wall carbon nanotube, Chem. Phys. Lett. 348 (2001) 187–193.